Elucidating the Structural and Minimal Protective Epitope of the Serogroup X Meningococcal Capsular Polysaccharide

Gian Pietro Pietri, Marta Tontini, Barbara Brogioni, Davide Oldrini, Stefania Robakiewicz, Pedro Henriques, Ilaria Calloni, Vera Abramova, Laura Santini, Suzana Malić, et al.

Elucidating structural and minimal protective epitope of serogroup X meningococcal capsular polysaccharide

Gian P. Pietri[1], Marta Tontini[2], Barbara Brogioni[2], Davide Oldrini[2], Stefania Robakiewicz[3], Pedro Henriques[3, 2], Ilaria Calloni[4], Vera Abramova[1], Laura Santini[2], **Suzana Malić**[1], Karmela **Miklić**[2]**, Berislav Lisnić**[1], Sara Bertuzzi[4], Luca Unione[4], Evita Balducci[2], Jérôme D. Ruyck[3], Maria Rosaria Romano[2], JESUS JIMENEZ-BARBERO[4], Julie Bouckaert[3], Stipan Jonjic[1], Tihana Lenac Roviš[1], Roberto Adamo[2*]

[1]University of Rijeka, Croatia, [2]GlaxoSmithKline (Italy), Italy, [3]Université de Lille, France, [4]CIC bioGUNE, Spain

Keywords

structural glycobiology, glycoconhugates, Vaccines, Neisseria meningitidis, capsular polysaccharide

Abstract

Word count: 226

Despite the considerable progress towards the eradication of meningococcal disease with the introduction of glycoconjugate vaccines, previously unremarkable serogroup X has emerged in recent years, recording several outbreaks through the African continent. Different serogroup X polysaccharide-based vaccines have been tested in pre-clinical trials, establishing the principles for further improvement. To elucidate the antigenic determinants of the MenX capsular polysaccharide, we generated a monoclonal antibody, and its bactericidal nature was confirmed using the rabbit serum bactericidal assay. The antibody was tested by inhibition enzyme-linked immunosorbent assay and surface plasmon resonance against a set of oligosaccharide fragments of different lengths. The epitope was shown to be contained within 5 to 6 repeating units. The molecular interactions between the protective monoclonal antibody and the MenX capsular polysaccharide fragment were further detailed at atomic level by saturation transfer difference NMR spectroscopy. The NMR results were used for validation of the in-silico docking analysis between the x-ray crystal structure of the antibody (Fab fragment) and the modelled hexamer oligosaccharide. The antibody recognizes the MenX fragment by binding all 6 repeating units of the oligosaccharide via hydrogen bonding, salt bridges and hydrophobic interactions. In vivo studies demonstrated that conjugates containing 5-6 repeating units can produce high functional antibody levels. These results provide an insight on the molecular basis of MenX vaccine-induced protection and highlights the requirements for the epitope based vaccines design.

Contribution to the field

Identification of glycan epitopes is key for vaccine design. Meningococcal serogroup X has emerged in recent years as cause of outbreaks, particularly in the African continent. Different serogroup X polysaccharide-based vaccines have been tested in pre-clinical trials, establishing the principles for further improvement, however no information on structural and immunogenic epitope is known for this polysaccharide. Here we generated a functional mAb against MenX capsular polysaccharide, and we characterized the interactions with polysaccharide fragments by inhibition enzyme-linked immunosorbent assay and surface plasmon resonance. The epitope was shown to be contained within 5 to 6 repeating units. The molecular interactions between the protective monoclonal antibody and the MenX capsular polysaccharide fragment were further detailed at atomic level by saturation transfer difference NMR spectroscopy. The NMR results were used for validation of the in-silico docking analysis between the x-ray crystal structure of the antibody (Fab fragment) and the modelled hexamer oligosaccharide. The antibody recognizes the MenX fragment by binding all 6 repeating units of the oligosaccharide via hydrogen bonding, salt bridges and hydrophobic interactions. In vivo studies demonstrated that conjugates containing 5-6 repeating units can produce high functional antibody levels. These results highlight the potential of structural glycobiology to guide vaccines design.

Funding statement

Ethics statements

Studies involving animal subjects
Generated Statement: The animal study was reviewed and approved by Italian Ministry of Health (Approval number n. 804/2015-PR)..

Studies involving human subjects
Generated Statement: No human studies are presented in this manuscript.

Inclusion of identifiable human data
Generated Statement: No potentially identifiable human images or data is presented in this study.

Data availability statement

Generated Statement: The datasets presented in this study can be found in online repositories. The names of the repository/repositories and accession number(s) can be found in the article/supplementary material.

Elucidating structural and minimal protective epitope

of serogroup X meningococcal capsular polysaccharide

1 **Gian Pietro Pietri[1], Marta Tontini[2], Barbara Brogioni[2], Davide Oldrini[2], Stefania**
2 **Robakiewicz[3], Pedro Henriques[2], Ilaria Calloni[4], Vera Abramova[1], Laura Santini[b], Suzana**
3 **Malić[1], Karmela Miklić[1], Berislav Lisnic[1], Sara Bertuzzi[4], Luca Unione[4], Evita Balducci[2],**
4 **Jérôme de Ruyck[3], Maria Rosaria Romano[2], Jesus Jimenez-Barbero[4,5,6], Julie Bouckaert[3],**
5 **Stipan Jonjic[1], Tihana Lenac Rovis[1*], Roberto Adamo[2*]**

6 [1]Center for Proteomics, Faculty of Medicine, University of Rijeka, Rijeka, Croatia

7 [2]GSK Vaccines, Via Fiorentina 1, 53100 Siena, Italy

8 [3]Unité de Glycobiologie Structurale et Fonctionnelle, UMR 8576 du CNRS et Université de Lille, 50
9 Avenue de Halley, 59658 Villeneuve d'Ascq, France

10 [4]Chemical Glycobiology Lab CIC bioGUNE Technology Park, 48160 Derio, Spain

11 [5]Ikerbasque, Basque Foundation for Science, 48013 Bilbao, Bizkaia, Spain

12 [6]Department of Organic Chemistry II, University of the Basque Country, Universidad del País
13 Vasco/Euskal Herriko Unibertsitatea, 48940 Leioa, Bizkaia, Spain

14

15 *** Correspondence:**
16 Corresponding Authors
17 tihana.lenac@uniri.hr; roberto.x.adamo@gsk.com

20 **Abstract**

21 Despite the considerable progress towards the eradication of meningococcal disease with the
22 introduction of glycoconjugate vaccines, previously unremarkable serogroup X has emerged in recent
23 years, recording several outbreaks through the African continent. Different serogroup X
24 polysaccharide-based vaccines have been tested in pre-clinical trials, establishing the principles for
25 further improvement. To elucidate the antigenic determinants of the MenX capsular polysaccharide,
26 we generated a monoclonal antibody, and its bactericidal nature was confirmed using the rabbit serum
27 bactericidal assay. The antibody was tested by inhibition enzyme-linked immunosorbent assay and
28 surface plasmon resonance against a set of oligosaccharide fragments of different lengths. The epitope
29 was shown to be contained within 5 to 6 repeating units. The molecular interactions between the
30 protective monoclonal antibody and the MenX capsular polysaccharide fragment were further detailed
31 at atomic level by saturation transfer difference NMR spectroscopy. The NMR results were used for
32 validation of the in-silico docking analysis between the x-ray crystal structure of the antibody (Fab

33   fragment) and the modelled hexamer oligosaccharide. The antibody recognizes the MenX fragment by
34   binding all 6 repeating units of the oligosaccharide via hydrogen bonding, salt bridges and hydrophobic
35   interactions. In vivo studies demonstrated that conjugates containing 5-6 repeating units can produce
36   high functional antibody levels. These results provide an insight on the molecular basis of MenX
37   vaccine-induced protection and highlights the requirements for the epitope based vaccines design.

38   **1   Introduction**

39   *Neisseria meningitidis* (Men) is a gram-negative encapsulated diplococcus, capable of producing
40   meningitis and sepsis in humans (1-3). Every year, thousands of cases and scores of deaths are recorded
41   around the globe. However, the sub-Saharan African meningitis belt is by far the most affected area in
42   the latest years (1, 4-8).

43   Most pathogenic Men are coated by a capsular polysaccharide (CPS) (9), as it improves colonization
44   through evasion of the host's immune system (10). Based on the chemical composition of the CPS,
45   Men is subclassified into twelve serogroups, being A, B, C, W, Y and X the most clinically relevant
46   ones (4, 11, 12). Men CPS itself is highly immunogenic and elicits bactericidal antibodies in adult
47   population (10), consequently, it has been widely used for the development of polysaccharide vaccines
48   (3, 10, 12, 13). More recently, Men CPS has been covalently linked to immunogenic protein carriers,
49   such as the chemically detofixied Diptheria or Tetanus Toxins (DT and TT, respectively) and the
50   nontoxic mutant of diphtheria toxin, Cross-Reacting Material 197 (CRM$_{197}$), to form glycoconjugates
51   (1). Men glycoconjugates based vaccines, such as Menactra, Menveo and Nimenrix (targeting MenA,
52   C, Y, W) (1, 4, 11), have overcome most of the limitations of using plain Men CPS, i.e. lack of memory
53   response, IgM-to-IgG maturation and ineffectiveness in children below 2 years of age (7, 11, 13-15).
54   Over the last years, a MenA-TT conjugate, MenAfriVac, has been introduced in the so-called
55   meningitis belt, leading to almost eradication of the disease (16).

56   MenX strains were first described in 1966 by Boris et al. (17, 18), yet, until recently, their association
57   with invasive disease was not on pair with the other disease-causing serogroups (3). However, in the
58   last years, several MenX outbreaks have been registered in the meningitis belt (6, 7, 12). The surge of
59   MenX has alerted the World Health Organization (WHO), reclassifying this serogroup as a major threat
60   (1). Particularly after the introduction of MenA mass immunization in Africa, serotype displacement
61   of MenA carriage has been suggested as a contributing factor for the increase of MenX incidence (1).
62   Alternatively (17), recent work from Ji et al showed that a MenX strain, isolated from a bacteremia
63   case in China, derived from a MenA strain due to a capsule switching event (3).

64   Considering the potential emergence of MenX related meningococcal disease, (1, 3) it is indisputable
65   that MenX disease possess a threat to global health, making the development of a vaccine a top priority
66   (3).

67   Several MenX vaccines are already in preclinical trials, using MenX PS as vaccine antigen as the
68   leading strategy (4). For example, a vaccine containing MenX CPS fragments conjugated to CRM$_{197}$
69   has been successful at preclinical stage (1). A classic polysaccharide-protein conjugate approach is
70   under investigation by the Indian Serum Institute for the development of a pentavalent *Men*ACXYW
71   vaccine (NmCV-5). Other modern strategies include the vaccines containing enzymatic and chemically
72   produced MenX oligosaccharides (OS) (2, 4).

2

73   The MenX CPS is composed by a repeating unit (RU) of N-acetylglucosamine-4-phosphate residues
74   held together by α-(1-4) phosphodiester bonds (4). While this RU structure was first confirmed by ^{13}C
75   NMR in 1974 (18, 19), little is known about the minimal antigenic determinant of the polysaccharide.

76   *In vivo* studies performed by Morelli et al. found that 3 RUs was the minimal antigenic portion of the
77   CPS capable of eliciting protective antibodies (1). A synthetic fragment of 4 RUs has been also tested
78   (11) in vitro, however these short lengths are considered suboptimal to elicit a robust immune response
79   compared to the polysaccharide-conjugate. Therefore, despite dynamic simulation studies have
80   hypothesized that 4RU could be the minimal epitope required for eliciting an immune response (14),
81   it is general belief that longer fragments might be required to mimic the *in vivo* response achieved with
82   conjugates of the native CPS (1, 5, 11). In this context enzyme based or combined chemo-enzymatic
83   approaches have been used to develop conjugate vaccines based on oligomers of around 11 RUs which
84   induced high levels of functional antibodies (2).

85   Despite these studies to investigate the potential of MenX polysaccharide in vaccine design, both
86   structural antigenic determinant and minimal immunogenic epitope of MenX CPS have not been
87   elucidated (11, 20). This minimal epitope is crucial to guide vaccine design particularly from synthetic
88   approaches, where its length should ideally be short enough for practical synthesis while keeping
89   representation of the native CPS conformation (14, 20, 21). Mapping interactions of glycans with
90   protective antibodies epitopes is becoming a powerful tool to select glycans for epitope focused
91   vaccines eliciting long lasting immunity and highly specific bactericidal antibodies (22). This principle
92   has been successfully applied at preclinical level to generate glycoconjugate vaccines against *Clostrium*
93   *difficile*, *S. pneumoniae,*Group B *Streptococcus*, and other bacteria (21, 23-25).

94   Herein, we isolated the first bactericidal monoclonal antibody against MenX polysaccharide and
95   through an integrated approach based on ELISA, Surface Plasmon Resonance and STD-NMR we
96   characterized its affinity towards the CPS and the positions involved in binding. The Fab was also
97   crystallized to generate an in-silico model for the recognition with MenX CPS. The information
98   generated from epitope mapping was utilized for the preparation of conjugates from different oligomer
99   lengths. Combined data on the antigenic determinant involved in mAb recognition and on the minimal
100   immunogenic portion support the notion that the minimal structural and immunogenic epitope of MenX
101   CPS is comprised of 5-6 RUs.

102

103   **2   Results**

104   **2.1   Selection and immunochemical characterization of a functional anti-MenX murine mAb**

105   The anti-MenX CPS monoclonal antibody (mAb), clone MenX.01, was obtained using
106   hybridoma technology. The glycoconjugate of *Neisseria meningitidis* serogroup X polysaccharide and
107   CRM_{197} carrier protein (MenX-CRM_{197}) was used as immunogen (Figure 1a). Several attempts to
108   immunize mice and obtain hybridoma cell lines were necessary to develop one monoclonal antibody
109   that specifically recognizes MenX polysaccharide. In total, close to 6000 supernatants were tested for
110   the binding assay on MenX polysaccharide (MenX-CPS) coated ELISA plates. Positive supernatants
111   were re-tested and in parallel, a cross-reactivity test was performed on an irrelevant meningococcal
112   glycoconjugate. This resulted in a single hybridoma cell line that secreted antibody specifically
113   recognizing MenX-CPS, which was a kappa IgG1 isotype/subtype. Next, a large scale mAb production
114   and purification was performed and the leading candidate, clone MenX.01, was purified from serum
115   free medium by using one step affinity purification, in milligram scale. The purified MenX.01 mAb
116   was tested against several structurally different polysaccharides to confirm the lack of cross-reactivity

117   between MenX CPS recognition and other bacterial carbohydrates (Figure 1b). The specificity of the
118   MenX.01 mAb was further confirmed by immunostaining of MenX- CRM_{197} conjugate and CRM_{197}
119   conjugated to Group B Streptococcus GBSII as control (Figure 1c), where the glycoconjugate MenX-
120   CRM_{197}, showed its typical band on SDS PAGE. The bactericidal activity of the new mAb MenX.01
121   was then assessed through rabbit complement mediated serum bactericidal assay (rSBA). This assay is
122   a surrogate of protection against Men disease (26) where it measures the vaccine-induced antibody
123   potential to induce killing of Men in presence of rabbit complement (4). The bactericidal activity of
124   the highly specific anti-MenX PS antibody, clone MenX.01, was tested in vitro. An rSBA titer of 1024
125   at 0.98 µg/mL demonstrated the recognition of live bacteria MenX strain Z9516 and the capacity of
126   triggering complement-dependent cytotoxicity by MenX.01 mAb.

127

128   **2.2   Conformational analysis of MenX capsular polysaccharide**

129   MenX CPS is a homopolymer composed of α-(1-4)-phosphodiester linked N-Acetyl glucosamines
130   (27). To understand if potential structural epitopes could be predicted, its conformational behavior and
131   dynamic features were studied in silico using a combined theoretical (quantum mechanics -QM- and
132   molecular dynamics -MD- calculations) and experimental (NMR) approach. Special attention was paid
133   to the different torsion angles that define the glycosidic linkages and to the geometry of the six-
134   membered rings.

135   First, to unravel the dynamic features at the glycosidic linkage of MenX capsular polysaccharide while
136   reducing the cost of the computational study, we performed a long (1.0 µs) MD simulations of the
137   simpler disaccharide (DP2) repeating unit, using the carbohydrate molecules specific GLYCAM06
138   force field, explicit solvent molecules and periodic boundary conditions as implemented in the Amber
139   biomolecular simulation package (28). The results of the MD simulation indicated that in explicit
140   water, the MenX DP2 assumes a typical *exo-syn* conformation around the ϕ torsion angle, which is
141   strongly stabilized by the *exo*-anomeric effect. The Ψ torsion angle largely populates the *syn*-
142   conformation ($\psi = -60°$), which is favoured by steric effects, although minor excursions to other
143   regions of the conformational map such as the *syn+* and *anti* conformations (+60°, 180° degree
144   respectively) are also possible. Instead, a higher degree of flexibility was observed for the α and β
145   torsion angles. Specifically, the α angle shows a broad minimum around 0° degree (-60° $\leq \alpha \leq$ +20°),
146   while β is characterized by a larger flexibility, with low energy minima at 180°, -60° and 60° degrees
147   (Figure 2A). Taken altogether, the results from the MD simulation shows that the energy profile for
148   MenX DP2 explores different conformations, which differ for the combination of the flexible dihedral
149   angles Ψ, α, and β, while keeping the ϕ torsion in the *exo*-anomeric conformation (Figure 2B).

150   The energy minima structures identified for the MenX DP2 disaccharide by the MD simulation were
151   further evaluated using a QM approach at the B3LYP/6-31++g(d,p) level of theory, using the Gaussian
152   09 suite of programs (29) to derive their expected NMR parameters that were compared to those
153   experimentally determined. In particular, the analysis of the scalar (J) coupling constants was used to
154   define the conformational distribution around the glycosidic linkage. The comparison between the

155 experimental derived J-couplings and the calculated values confirmed the predominance of the *exo-*
156 *syn* (ϕ = 60°) over the *exo-anti* (ϕ = -60°) conformation, which is probably present as minor
157 conformation (Table S1, Supplemental Information). In agreement with the MD simulations previously
158 described, the QM data also support the coexistence of different populations for the β torsion angle,
159 while α is more restricted (-50° ≤ α ≤ 0°) (Table S3, Supplemental Information).

160 Next, the identified structure of the DP2 disaccharide in its low energy conformation was used to build
161 a longer dodecasaccharide fragment (DP12), as model of the entire polysaccharide. After submitting
162 the DP12 to 1.0 µs MD simulation, results recapitulated those obtained for the simpler disaccharide
163 with a few differences worth of mentioning. Briefly, the *exo-syn* conformation is preserved along the
164 entire simulation. The ψ dihedral angle mainly populates the *syn-* (-60°) geometry, with minor
165 excursions to the *syn+* (+60°) and *anti* (±180°) regions. A similar behaviour for α and β dihedral angles
166 is observed independently from the number of repeating units. Representative φ/ψ and α/β plots for
167 DP12 are reported in Figure 2C. The analysis of the puckering of the six-membered rings showed that
168 the low energy $^4C_1$ ring conformation is adopted by all residues along the entire simulation (data not
169 shown). Overall, while a recent study has hypothesized that MenX CPS could display a large
170 population of a helix-like geometry, especially for long polysaccharides, (14) the calculations
171 performed herein for DP12 predict the existence of conformational flexibility mainly governed by the
172 variability of β (mainly) and ψ, in a minor extent.

173

174 **2.3   Selection of MenX CPS fragments for structural studies**

175

176 The *in silico* analysis showed that MenX oligosaccharides display flexibility around the different
177 torsional angles. Starting from this basic information provided by the calculations, the minimal MenX
178 CPS portion able to recognize the functional MenX.01 mAb (30) was empirically determined. We
179 produced oligomers of different lengths, i.e. average degree of polymerization (avDP) starting from
180 the CPS. Mild acid hydrolysis and reaction monitoring by ^{31}P NMR spectroscopy allowed to obtain
181 the fragments (Figure S1-2). From the final sample with avDP 11.7 we purified oligosaccharide (OS)
182 fragments in the DP range from 1 to 11 (Figure 3a).

183 Competitive ELISA assay was carried out using different concentrations of the generated OS fragments
184 (DP5.5–40 range) as inhibitors. MenX.01 mAb was incubated with increasing amounts of different OS
185 fragments and later transferred to MenX CPS immobilized on ELISA plates (Figure 3b). Absence of
186 primary antibody was used as negative control. Inhibition of mAb at shorter lengths was comparable
187 between DP5.5, DP8 and DP10.5. The inhibition was increased by 0.5 log with DP15 and by 1 log
188 with DP40 fragment, the later was slightly increased with the CPS. Therefore, competitive ELISA with
189 the newly developed bactericidal MenX.01 mAb confirmed length-dependent recognition of the
190 different fragments, that is, shorter fragments inhibited the interaction only at higher concentrations.
191 The results also showed that avDP5.5 OS was sufficient to fully inhibit the binding of the mAb to the
192 native CPS, thus containing the minimal epitope. This is in line with previous reports showing that 4

193 RUs were not sufficient to inhibit the binding of rabbit anti MenX specific serum, unless exposed as
194 protein conjugate (11).

195 To measure the binding kinetics of MenX.01 mAb and to examine its binding to shorter DP fragments,
196 additional studies were performed using Surface Plasmon Resonance (SPR). For this purpose, an
197 avDP15 MenX conjugated to CRM_{197} was immobilized on a CM5 chip via the EDC chemistry (pH 5)
198 at a level of 458 RUs. The interaction was fit through the 1:1 Langmuir binding model. The equilibrium
199 constant K_d (µM) of $0.32 \pm 0.04 \times 10^{-6}$ fitted based on the kinetic constants $k_a = 8.64 \times 10^3$ $M^{-1}.s^{-1}$, $k_d =$
200 2.75×10^{-3} s, indicates a submicromolar affinity of the antibody for the MenX polysaccharide presented
201 as a CRM_{197}-conjugate Figure 3c). The SPR kinetic analysis of the MenX.01 mAb showed that it binds
202 with relatively fast on- and off-rates and moderate affinity to MenX, as typical for low affinity
203 carbohydrate-protein interactions. In a competitive SPR study, we confirmed that DP5.5 retains an
204 almost complete (75%) capacity to block MenX.01 binding, compared to CPS (Figure 3d). On the
205 other hand, the minor fragment (DP2) had a very weak inhibitory capacity.

206 To gain further insights on the impact of carbohydrate length on binding, isothermal titration
207 calorimetry (ITC) of OS in complex with the MenX0.1 mAb was performed. The obtained data
208 indicated that the affinity for the MenX.01 mAb was very similar for DP5.5, 7 and DP9 (Table S3 and
209 Figure S4, Supplemental Information), confirming that 5-6 RUs are sufficient to strongly bind to the
210 mAb. The interactions of the antibody with MenX fragments appeared largely entropically driven, with
211 only a small enthalpic contribution. The affinity (K_d) varied from ~2-3 µM for the smaller DP5.5-7, as
212 measured by ITC, to ~0.3 µM, as determined for avDP15 by SPR (Table S3 Supplemental Information
213 and Figure 3c, respectively).

214

2.4 Mapping of the MenX antigenic determinant by STD-NMR

216 Considering that above a length of 5-6 RU the capacity to bind to antibodies was similar to the
217 CPS, the interaction of the DP7 and the mAb MenX.01 was investigated by STD-NMR to map
218 positions involved in binding. The ^{1}H NMR spectrum is characterized by a distribution of the ring
219 protons within a small range of chemical shifts, which renders possible to make only qualitative
220 considerations. Following irradiation of the DP7-mAb complex at 7 or 8 ppm, it clearly appeared that
221 all the protons from MenX repeating unit were receiving transfer of saturation (Figure 4), and
222 particularly the positions H-1 and H-4 which are held together by the phosphodiester bridge connecting
223 the proximal units. This indicates that the area surrounding these charged groups is likely involved in
224 strong interactions with the binding pocket. Since the hydrogen atoms of the GlcNAc residues in the
225 typical $^4C_1$ chair conformation point towards different spatial directions, the observed STD NMR
226 response is the result of overall contribution of the different sugar units along the DP7 chain.

227

6

228

229 **2.5   MenX.01 Fab X-Ray Crystallography**

230   To determine the exact binding epitope of MenX.01 antibody on MenX sugar, we approached
231 co-crystallization studies. For crystallization purposes, we produced different types of Fab fragments:
232 Fab enzymatically obtained by digestion of MenX.01 IgG1 antibody with papain and recombinant
233 Fabs, with and without His tag, by production in transiently transfected HEK293T cells. All the three
234 Fab fragments were successfully purified and functional (the enzymatic Fab and the recombinant His
235 Fab shown in Figure S3A-D), but none yielded crystals in co-crystallization studies. Then we produced
236 a fourth Fab - IgG2a recFab-His. Functionality and an affinity close to that of the original MenX.01
237 antibody was demonstrated for this Fab (Figure S5, Supplemental Information). Co-crystallization
238 studies of IgG2a recFab-His with the first smaller fragment of DP4 yielded crystals for X-ray analysis
239 which diffracted at a resolution of 2.16 Å (Figure S6, Supplemental Information). Unfortunately, the
240 crystals contained Fab alone and not of the Fab-DP4 complex. Attempts to soak the crystals with
241 millimolar concentrations of DP5.5 and DP4 were without success. Therefore, the obtained crystal was
242 used for docking studies as confirmation of the NMR data.

243

244 **2.6   In Silico docking studies of MenX OS complexed with the mAb**

245   To gain further insights into the molecular basis of recognition, the MenX hexasaccharide
246 (DP6) was docked into the carbohydrate recognition domain (CRD) of the Fab region of the MenX.01
247 mAb. The DP6 structure, corresponding to the central section of the DP12 obtained by the MD
248 simulations, was used as representative of the DP5.5 MenX minimal epitope (Figure 5). The CRD of
249 the MenX.01 mAb shows an extended U-shaped groove running from the heavy to the light chains.
250 Interestingly, most of the residues composing the CRD are positively charged amino acids (K5, R31,
251 K75, K81, R97, R100 in the heavy chain, and K45, R55 in the light chain), which confer a high positive
252 charge to the surface (Figure S7, Supplemental Information). Fittingly, the negatively charged
253 phosphate groups of the MenX DP6 may, at least partially, satisfy the positively charged surface. Thus,
254 the DP6 was docked into the CRD guided by the possible electrostatic intermolecular interactions
255 among those groups. Next, a docking-minimization protocol of the complex was performed using the
256 MAESTRO (Schrödinger) suite of programs (31). According to the calculations, the complex was
257 conformationally stable and most of the intermolecular interactions were maintained, while new ones
258 where found. In details, R31 and R100 establish electrostatic interactions with the phosphodiester
259 groups at the termini of the oligosaccharide chain. Additionally, all six residues of the DP6 participate
260 in hydrogen bond intermolecular interactions. In total, 9 hydrogen bonds within residues S33, N98,
261 Y99, R100, G101, G26 and E50 stabilize the complex, with four of them mediated by the
262 phosphodiester groups all along the carbohydrate chain (Figure 5). Finally, non-polar patches from the
263 aromatic side chins of residues W52, Y99, Y32 and F27 also provide hydrophobic interactions to the
264 DP6 oligosaccharide (Figure 5c). Interestingly, the phosphodiester groups at the edges of the DP6
265 oligosaccharide are instrumental to anchor the oligosaccharide chain to the mAb CRD through salt
266 bridges with the R31 and R100 residues, at the termini of the CRD. Additionally, the internal sugar
267 residues establish a variety of intermolecular interactions all along the extended groove. This

268   interaction pose is agreement with the STD NMR outcome, which suggested that DP6 is globally
269   involved in mAb recognition.

270

271   **2.7   Immunogenicity studies**

272   In order to study the impact of the saccharide chain length on the sugar immunogenicity and
273   assess whether the 6-mer identified as putative minimal epitope was able to elicit a robust and
274   protective immune responses, the DP5.5, 10 and 20 fragments were conjugated to CRM_{197} to be tested
275   in mouse animal model. Conjugation of MenX OS was achieved through a three-step procedure
276   involving (i) reductive amination with a di-hydrazine linker to insert a hydrazine moiety and (ii)
277   following reaction with di-N-hydroxysuccinimidyl adipate to transform the compound in a half ester
278   for (iii) final coupling to the protein carrier. The obtained conjugates were characterized to determine
279   the saccharide/protein ratio by protein and saccharide content determination, and the molecule profile
280   by SDS-page and HPLC (Figure S8, Supplemental Information).

281   The prepared glycoconjugate vaccines were administered to mice at days 1, 14, 28 using a 1
282   µg/saccharide of each biomolecule. Sera sampling was collected 14 days after the second and the third
283   dose. Sera were analyzed for anti-MenX PS IgG content by ELISA and for antibody functionality by
284   SBA.

285   All the vaccines were able to induce a specific antibody response against the native MenX PS
286   after the second dose that was boosted with the third dose (Figure 6). The DP5.5 was able to induce
287   IgG levels comparable to the conjugated DP10, and with similar functional activity, clearly indicating
288   that this sugar length represents the minimal epitope capable of inducing a strong immune response.
289   The conjugated DP20 induced the best response from the set in terms of both antibodies and SBA titers,
290   highlighting that further optimization of the immune response can be obtained by long fragments as
291   result of the multiple exposition of the minimal epitope along the polysaccharide chain.

292

293   **3   Discussion**

294   In this study, we developed a highly specific antibody against MenX polysaccharide, clone
295   MenX.01 which is showed to be bactericidal. Our structural and immunogenicity data converged
296   establishing that MenX minimal epitope is contained within 5-6 RUs (DP5.5).

297   To our knowledge, currently there is only one monoclonal antibody, mAb 10B5F10, previously
298   developed by Reyes et al. (32), that recognizes MenX CPS, whose bactericidal activity, however, was
299   not assessed. Our bactericidal mAb is an IgG1 subtype, which could be connected to the dominance of
300   this subclass production induced by alum adjuvanted vaccination with glycoconjugates (33, 34).   8

301

302   MenX.01 mAb was able to induce bactericidal killing at a concentration as low as 1 µg/mL
303   (rSBA of 1024). An rSBA titer of ≥8 has been accepted as the correlate of protection for Men protective
304   sera (35), however SBA protection threshold has not been defined for purified mAbs. Nevertheless,
305   this protective mAb concentration seems realistic within the normal range of IgG in plasma, since other
306   immunization studies in mice using pneumococcal conjugates have produced specific anti-PS IgG
307   antibody concentrations in sera of ~10 µg/mL (36). Moreover, we found our rSBA titer similar to the
308   anti-MenA PS mAb 7E1F7, which reported rSBA titers in the range of 0.49 to 0.122 µg/mL (37).
309   Altogether, this is evidence that the produced mAb is bactericidal at physiological IgG concentration
310   in sera.

311   In the case of homopolysaccharides, such as MenX CPS, identification of the conformation
312   and orientation of the bound epitope to the corresponding antibody is challenging (38). Therefore, the
313   first step was to have an estimate of the shortest OS which contained the minimal antigenic determinant
314   for further characterization. In our competitive ELISA study, OS fragment avDP5.5 achieved full
315   inhibition of the mAb-CPS binding. Furthermore, longer fragments, DP8 and DP10/11, did not increase
316   the inhibition. This is an indication that the binding epitope is preserved above 5 RU. Shorter OS
317   fragments, such as DP4, could be considered suboptimal epitopes. The higher inhibition observed with
318   DP15 and larger fragments is most probably due to a multivalency effect. These longer fragments
319   support multiple binding to their repeated epitopes, while no specific conformational structure could
320   be predicted in silico for MenX CPS, SPR differences in the K_a/K_d values from mAb and Fab
321   highlighted that an avDP5.5 was able to bind to the mAb similarly to the CPS.

322   Of the range of Fab fragments that we successfully produced and purified, only recombinant
323   Fab-IgG2a-His yielded crystals. Co-crystallization with sugar fragments proved to be unsuccessful
324   (38). In silico prediction on the MenX CPS conformation showed a high degree of flexibility in the
325   polymer which prevents the formation of a preferential secondary structure, as opposed as a recent
326   study highlighting potential formation of a helical structure for a length above 6 RU (14). Docking
327   studies with a 6 RU fragment and the crystal structure of the Fab along with STD NMR analysis showed
328   that indeed this length is sufficient to fully occupy the binding pocket. A network on hydrogen bonds
329   involving the charged phosphate groups along with additional non polar patches would play a relevant
330   role in stabilizing such interactions.

331   Finally, the identified epitope recognized by the functional mAb was conjugated to a carrier
332   protein demonstrating to elicit an immune response similar to a longer avDP10. This clearly indicates
333   that a length of 5-6 RU contains the minimal epitope of MenX CPS. The functional antibody levels
334   were further increased for a conjugated avDP20 as result of multimeric presentation of the identified
335   epitope.

336   In conclusion, our work identified a length of 5-6 RU as minimal structural and immunogenic
337   epitope of MenX capsular polysaccharide. Further effort will be devoted to unravel fine details of the
338   recognition of functional antibodies. This study highlights the importance of a structural approach for
339   the rational selection of the polysaccharide fragments for vaccine development. In addition, this study
340   can guide the design of minimal epitope based vaccines using synthetic or enzymatic methods.

341

4 Materials and Methods

4.1 Development of the anti-*Neisseria meningitidis* serogroup X polysaccharide (MenX-CPS) monoclonal antibody, clone MenX.01

The glycoconjugate of *Neisseria meningitidis* serogroup X polysaccharide with CRM_{197} carrier protein (MenX-CRM_{197}) (GSK, Siena, Italy) was used for BALB/c mice immunization (in groups of 3 mice). Immunogens were prepared by mixing MenX-CRM_{197} stock (2 µg polysaccharide content, diluted in phosphate buffer saline), with Alhydrogel® adjuvant 2% (aluminium content: 9-11 mg/ml) in 1: 9 alhydrogel: MenX-CRM_{197} ratio. The immunogen was prepared on the day of immunization and gently mixed at RT for 4-5 hours. Mice were subcutaneously immunized with MenX-CRM_{197} conjugate and Alhydrogel® adjuvant two times, at day 0 and 14. After second immunization, the sera of immunized BALB/c mice were screened for antibody titers against the MenX polysacharide (MenX CPS) (GSK, Siena, Italy) by using an enzyme-linked immunosorbent assay (ELISA) using plates coated with the respective polysaccharide. The mouse with the highest MenX titer was boosted one more time with the immunogen. Three days later, spleen cells were collected and, after lysis of red blood cells, fusion with SP2/0 myeloma cells at ratio 1:1 was performed. In total, 70 million lymphocyte cells were fused with 70 million fusion partner cells and plated on 6x 96-well plates. These hybridoma cell lines were cultured in 20% RPMI 1640 medium containing hypoxanthine, aminopterin, and thymidine for hybridoma selection. Cell growth was examined 2 weeks after fusion. In the first test, supernatants were screened by ELISA against MenX CPS and 18 positive hybridoma-motherwells were further propagated. The hybridoma-motherwells were retested next day and those with the retained positivity against MenX CPS (7 out of 18) were subsequently expanded and cloned by limiting dilution. Obtained cell lines were cultured and retested for their positivity against i) MenX-PS, ii) MenX-PS-CRM_{197} conjugate, iii) Protein carrier, CRM_{197} (GSK, Siena, Italy), iv) an irrelevant polysaccharide antigen, Group B streptococcus type II (GSK, Siena, Italy), and v) another irrelevant polysaccharide antigen, a meningococcal antigen, *Neisseria meningitidis* serogroup A polysaccharide (MenA-CPS) (GSK, Siena, Italy). Only one hybridoma-motherwell resulted in the antibody with the desired characteristics. Other attempts to obtain monoclonal antibodies against MenX CPS using 8 mice, with minimal variations in the immunzation protocol, did not yield additional antibody clones. Therefore, we generated one monoclonal antibody that specifically recognized MenX-PS and named it clone MenX.01. Large scale MenX.01 production was performed in RPMI 1640 media (PAN-Biotech GmbH) supplemented with FBS standard (PAN-Biotech GmbH) (10%), penicillin-streptomycin (PAN-Biotech GmbH) (final concentrations: penicillin 10 U/mL; streptomycin 10 µg/mL), L-Glutamine (PAN-Biotech GmbH) (final concentration: 0.2 mM) and β-Mercaptoethanol 50 mM in PBS (PAN-Biotech GmbH) (final concentration: 5 µM). The mAb was purified from the culture supernant, using GE AKTA Pure Liquid Chromatography System and HiTrap Protein G HP prepacked columns for preparative purification of monoclonal antibodies, in an amount of few milligrams.

10

4.2 Enzymatic Fab production

379 Affinity-purified MenX.01 mAb was concentrated to 2 mg/mL in PBS and cleaved into Fab and Fc
380 fragments according to the protocol of Andrew & Titus (39). Briefly, purified antibody stock in PBS
381 (2 mg/ml) was dissolved in freshly prepared 2x digestion buffer (0.035 M EDTA, 40 mM L-cysteine
382 in PBS). Freshly prepared papain (0.1 mg/ml) was mixed in a 1:1 ratio with the antibody in 2x digestion
383 buffer and incubated (37 °C, 2 hours). The reaction was stopped by the addition of iodoacetamide to a
384 final concentration of 30 mM. The Fab fragment was purified from papain, Fc fragment and the
385 undigested IgG on ÄKTA FPLC via tandem Protein G and Protein A affinity purification. Fab
386 fragments were then concentrated in PBS centrifugal Amicon-filter concentrators (molecular weight
387 separation 10 kDa) (Merck KGaA) to a final concentration of 1 mg/ml. The purity of the Fab was
388 confirmed by SDS-PAGE analysis followed by SDS-PAGE and western blot/immunoblot analysis
389 CPS (S Figure S3a-b).

390 **4.3   Recombinant Fab production**

391 The construction of the plasmids for recombinant Fab expressions were obtained by sequencing,
392 synthesis and cloning by GenScript USA Inc. (New Jersey, USA). Briefly, from the selected hybridoma
393 clone, RNA was reverse transcribed into cDNA. The antibody fragments of variable heavy chain (V_H)
394 and variable light chain (V_L) were amplified, cloned into a standard cloning vector separately. Colony
395 PCR was performed to screen for clones with inserts of the correct sizes and no less than five colonies
396 with the correct insert size were sequenced. The resulting sequence is the consensus derived from the
397 alignment of these clones (S, sequences).

398 The antibody fragment of V_H was synthesized and fused with either the IgG1 or the IgG2a first constant
399 heavy chain domain (C_H1), the later was also designed to contain a 6x histidine tag at the C-terminal
400 region. The V_L was processed similarly with the IgG constant kappa light chain domain (CL). The
401 synthesized IgG1/IgG2a-kappa heavy and light chains were cloned separately into mammalian
402 expression vector pcDNA3.4.

403 Transient expression of recombinant Fab was performed in either mono, tri or five-layer cell culture
404 flask (Corning™ Falcon™ Fischer Scientific). HEK293T cells in RPMI 1640 media (PAN-Biotech
405 GmbH) supplemented with FBS standard (PAN-Biotech GmbH) (10%), MEM NEAA (100x) (PAN-
406 Biotech GmbH) and sodium pyruvate (PAN-Biotech GmbH) (final concentration 0.1 mM) were seeded
407 24 hours before transfection in order to achieve an 80% confluency next day. For each flask layer, the
408 transfection mixture was prepared by mixing 19 μg of each heavy and light chain purified plasmids,
409 185 uL of polyethylenimine (PEI) solution (1 mg/mL) and 2.8 mL of DMEM media (PAN-Biotech
410 GmbH) for 20-30 min at RT. Next, the flask media was removed, and the transfection mixture was
411 added, after incubating for 2 minutes, the media was returned to the culture flask and the flask was
412 placed back in the incubator. After 24 h, the media was exchanged with HyClone™ HyCell TransFx-
413 H Medium (Cytiva, previously GE Healthcare) supplemented with MEM NEAA (100x) (PAN-Biotech
414 GmbH), sodium pyruvate (PAN-Biotech GmbH) (final concentration: 0.1 mM), penicillin-
415 streptomycin (PAN-Biotech GmbH) (final concentrations: penicillin 10 U/mL; streptomycin 10
416 μg/mL)and L-Glutamine (PAN-Biotech GmbH) (final concentration: 0.2 mM). Media was collected
417 and replaced every 3-5 days for 1-2 weeks. The recombinant mouse Fabs were purified from the

418 supernatant using GE AKTA Pure Liquid Chromatography System equipped with a HisTrap HP
419 columns packed with Ni Sepharose affinity resin. The Fab was analyzed by ELISA and western blot
420 to confirm specific binding to MenX CPS (Figure S3c-d).

421 **4.4 ELISA**

422 Microtiter plates (96 wells, MICROLON® High Binding, Greiner Bio-One) were coated with
423 polysaccharides (MenX-PS, MenA-PS, GBSII-PS), glycoconjugate MenX-CRM$_{197}$ or CRM$_{197}$ protein.
424 100 µL of CPS (5 µg/mL) in PBS pH 8.2 or 50 µL glycoconjugate/protein (2 µg/mL) in coating buffer
425 pH 9.6 was added in each well. Plates were incubated overnight at 2-8 °C, washed two times with tap
426 water and saturated with 150 µL/well PBST-B (3.0% Bovine Serum Albumin-BSA in PBST (0.05%
427 Tween-20 in PBS pH 7.4)) for 1 hour at 37°C. The plates were flicked off to remove the solution and
428 washed twice with tap water. The coated plates were incubated with mAb or Fab thereof in various
429 dilutions, at room temperature for 1 hour, washed twice and incubated for 1 additional hour at room
430 temperature with either anti-mouse IgG (H+L) Fc peroxidase (Jackson ImmunoResearch) diluted
431 1:1000 or anti-mouse IgG F(ab')$_2$ peroxidase (Jackson ImmunoResearch) 1:1000 diluted in PFT (1%
432 FCS in PBST). After washing six times, the plates were developed with a 0.6 mg/mL solution of o-
433 phenylenediamine dihydrochloride (OPD) (Sigma) in citrate buffer pH 5.5 and 0.001% of 30%
434 hydrogen peroxide, at room temperature for 5-10 min. After stopping the reaction with 1M sulfuric
435 acid, the absorbance was measured using a TriStar LB 941 multimode microplate reader with
436 wavelength set at 490 nm and reference filter set at 630 nm. ELISA inhibition experiments were
437 performed following the same procedure but pre-incubating the samples with one or more
438 concentrations of the inhibitor for 20 min at room temperature.

439 **4.5 Western blot/immunoblot analysis**

440 CRM$_{197}$ protein or MenX-CRM, MenA-CRM$_{197}$ and GBSII-CRM$_{197}$ glycoconjugates, in the amount
441 of 2-10 µg, were separated by 8% SDS-PAGE electrophoresis. Fab fragments, in the amount of 2-10
442 µg, were separated on 10-12% SDS-PAGE electrophoresis. Samples were transferred onto 0.45 µm
443 PVDF membrane (Hybond™, GE Healthcare) which were subsequently blocked with 5% w/v blotting
444 grade low fat powdered milk (Carl Roth Gmbh & Co. Kg). Membranes were incubated with clone
445 MenX.01 (mAb or Fab) overnight at 4°C. We used our own stock antibodies at a concentration of 1
446 mg/ml with a typical dilution of the primary antibody being 1:100. Protein signals were developed
447 using anti-mouse IgG F(ab')2 peroxidase (Jackson ImmunoResearch) 1:1000 and visualized with an
448 ImageQuant LAS 4000 mini camera system (GE Healthcare). Fab fragments were developed with
449 either anti-mouse IgG F(ab')2 peroxidase (Jackson ImmunoResearch) diluted 1:1000 or anti-mouse
450 IgG (H+L) Fc peroxidase (Jackson ImmunoResearch) diluted 1:1000 to confirm the absence of the Fc
451 fragment in the preparation.

452 **4.6 Complement-Mediated Bactericidal Activity (Rabbit Serum Bactericidal Activity Assay)**

453 Serum bactericidal activity against *N. meningitidis* serogroup X strain Z9516 was evaluated as reported
454 elsewhere (40), with minor modifications. Briefly, bacteria were grown overnight on chocolate agar
455 plate (Biomerieux 43101) at 37°C in 5% CO$_2$. Colonies were inoculated in 7 ml of Mueller–Hinton

12

456 broth containing 0.25% glucose to an optical density at 600 nm (OD_{600}) of 0.05-0.06 and incubated at
457 37°C with shaking until early log phase [OD_{600} of ~0.25 corresponding to 10^9 colony-forming units
458 per ml (CFU/ml)]. The cultured bacteria were diluted in Dulbecco's Phosphate Buffered Saline (DPBS-
459 SIGMA D8662) containing 1% bovine serum albumin (BSA)(Sigma) and 0.1% glucose at the working
460 dilution of 10^4-10^5 CFU/ml. The SBA was run in round bottom 96 well microplates in a final volume
461 of 50 μl per well with 25 μL of serial two-fold dilutions of test sample (mAb and polyclonal Abs), 12.5
462 μL of bacteria at the working dilution, and 12.5 μL of active complement (25%). The bactericidal assay
463 contains two internal controls: the first, to evaluate the bacterial killing by complement alone in the
464 absence of antibodies, the second to evaluate the killing by serum alone in presence of heat inactivated
465 complement. The reaction mixtures were incubated at 37°C for 60 minutes with 5% CO_2, then each
466 sample was spotted on Mueller–Hinton agar plates. Serum bactericidal titers were defined as the mAb
467 concentration resulting in 50% decrease in CFU/ml after a 60-min incubation of bacteria with the
468 reaction mixture compared to the control CFU/ml at time zero.

469 **4.7   Fragments of MenX polysaccharide preparation by mild hydrolysis**

470 The DP40 OS depolymerization was performed by mild acid hydrolysis. A phosphodiester bond links
471 *N. meningitidis* capsule building blocks, and the hydrolysis of this bond gives rise to a
472 phosphomonoester bond. Therefore, measuring the ratio from the mono and diester bond is a way of
473 following the hydrolysis reaction and estimate of the average degree of polymerization (DP) of the
474 sample. The process was monitored by phosphorus (^{31}P) NMR spectroscopy, and it was quenched by
475 neutralization when the desired average degree of polymerization (avDP) was reached. For a MenX
476 OS target of avDP 5, the hydrolysis was performed in 50 mM NaOAc with saccharide concentration
477 of 2.5 mg/mL at pH 4.0 and 80 °C, for ~18 h and two times overnight at RT. The reaction was quenched
478 by neutralization with NaOH when ^{31}P NMR indicated an avDP of 11.7.

479 **4.8   Purification of oligosaccharides**

480 The fragments of different lengths were separated by anionic exchange chromatography using a
481 semipreparative HPLC with a Sepharose Q column. By increasing the NaCl percentage of the elution
482 buffer with a linear gradient, it was possible to isolate every oligosaccharide fragment in the range of
483 1-11 repeating units.

484 The length of the oligosaccharides was determined by ^{31}P NMR analysis. The ^{31}P NMR signals of
485 phosphodiester in chain groups (P_{Int}) and phosphomonoester end groups (P_{Ter}) were integrated and used
486 for avDP calculation:

$$avDP = \left[\left(\frac{P_{Int}}{P_{Ter}}\right) + 1\right]$$

488 MenX OS's were desalted against water on a SEC Sephadex G-10 column (~0.3 mg of OS loaded per
489 1 mL of resin at 30 cm/h.

490 **4.9   Surface Plasmon Resonance (SPR) analysis**

491 Binding kinetics and affinities were determined by SPR using a BIACORE X100 system.
492 Glycoconjugates of MenX were immobilized on research grade CM5 sensor chips (Biacore) using the
493 amine coupling kit supplied by the manufacturer (Biacore). Immobilizations were conducted in 10 mM
494 sodium acetate (pH 5) at sugar concentration of 30 µg/mL. The immobilized surface density was ~500
495 resonance units in each instance. Measurements were conducted in PBS Tween20 0.005% pH=7.2 at
496 25°C and at a flow rate of 45 µL/min. Following mAb or Fab binding, conjugate surfaces were
497 regenerated with 3.5 M MgCl$_2$ and a contact time of 120 s. Sensorgram data were analyzed using
498 BIAevaluation software (Biacore). For competitive SPR PBS Tween 0.005% pH=7.2 was used as the
499 running buffer for the inhibition assays, at a 45 µl/min flow rate at 25°C. The experiment started with
500 three start-up cycles to allow surface stabilisation. Each sample injection (120 s contact time, 300 s
501 dissociation time) is followed by regeneration with 3.5 M MgCl2 (120 s contact time) to remove the
502 bound analyte from the ligand immobilised on the chip surface. 10 µM MenX mAb MenX.01 has been
503 used together with descending concentrations of MenX CPS, DP5, and DP2 (500 µg/mL, 250 µg/mL,
504 125 µg/ml, 62.5 µg/mL, 31.3 µg/mL, 15.6 µg/mL, 7.8 µg/mL, 3.9 µg/mL, 2 µg/mL, 1 µg/mL, 0.5
505 µg/mL, 0 µg/mL (no analyte in the mAb solution)).

4.10   Isothermal Titration Calorimetry (ITC) measurement

507 ITC experiments were performed with different concentrations of MenX.01 antibodies (~ 3, 6, 7 and
508 10 µM), at different temperatures (18°C, 25°C) and with different buffers (HEPES, PBS). The best
509 results are obtained with 10.9 microM mAb and at 25°C in HEPES. For each of the MenX fragments
510 DP7 and DP5.5, min 3 experiments were performed at different molar concentrations of the analyte.

4.11   STD NMR experiments

512 The interactions of the mAb MenX0.1 with DP7 in 1:50 molar ratio was studied by Saturation Transfer
513 Difference (STD)-NMR using the pulse sequence from the Bruker library (stddiffesgp.3). Spectra were
514 recorder at a 600 MHz at room temperature with 64 scans repeated in 64 loops in a matrix of 32k points
515 in t2 in a spectral window of 6692.11 Hz centered at 2820.00 Hz. Excitation sculpting with gradients
516 was employed to suppress the water proton signals. A spin lock filter (T1p) with a 2 kHz field and a
517 length of 30 ms was applied to suppress protein background. Selective saturation of the protein
518 resonances was performed by irradiating at 7.0 ppm (on resonance spectrum) using a series of shaped
519 90° pulses (50 ms, 1 ms delay between pulses) for a total saturation time of 2.0 s. For the reference
520 spectrum (off resonance spectrum), the irradiation took place at 30 ppm. To obtain the 1D STD-NMR
521 spectra the on-resonance spectra was subtracted from the off-resonance using Topspin 2.2 software.
522 The difference spectrum corresponds to the STD-NMR spectrum and the intensity of its signals is
523 proportional to the proximity of the corresponding protons to the protein. The STD was analysed using
524 the amplification factor (A_{STD}). The amplification factor is obtained by multiplying the relative STD
525 effect of a given proton (I_{STD}/I_0) at a given ligand concentration ($[L]_T$) with the molar ratio of ligand in
526 excess relative to the protein ($[L]_T/[P]$), according to Equation

14

527
$$ASTD = \frac{I_0 - I_{SAT}}{I_0} \, X \, \frac{[L]_T}{[p]} = \frac{I_{STD}}{I_0} \, X \, \frac{[L]_T}{[p]}$$

528   Were A_{STD} is the STD amplification facto, I_0, I_{SAT} and I_{STD} are the intensities of the reference (off

529   resonance spectra), saturated (on resonance spectra) and difference spectra, respectively. In order to

530   get the epitope mapping information from the amplification factor, the relative A_{STD} with the highest

531   intensity is set for 100%, and all the other signals are normalized accordingly.

532   4.12   Ab initio calculations

533   DFT calculations were carried out with the Gaussian 09 suite of programs. The geometry optimization

534   and the scan analysis were performed utilizing Becke's hybrid three-parameter exchange functional

535   and the nonlocal correlation functional B3LYP with the 6-31++g(d,p) basis set. Solvent effects were

536   included using the polarizable continuum model (PCM) for water (IEF-PCM). Electronic energies were

537   used to derive the energy profiles around the dihedral angles of interest (φ/ψ and α/β). Scalar coupling

538   constants were computed for all the possible conformations (*exo-syn*, non-*exo* and *exo*-anti around φ,

539   and gg, gt and tg around ω) using the GIAO method.

540   4.13 Molecular Dynamics Simulations

541   1 µs MD simulations of MenX DP2 and DP12 were performed using the AMBER12 and AMBER16

542   force fields within GLYCAM06 in explicit water. MenX DP2 and DP12 molecules were built using

543   the GLYCAM carbohydrate builder web tool (http://glycam.org). The phosphate linkers were added

544   using the xleap module of AMBER12 and the parameters and partial atomic charges were calculated

545   with the antechamber module (derived from the DNA phosphodiester bond) using GAFF force field.

546   The resulting geometries were extensively minimized using conjugate gradients and then taken as

547   starting structures for the MD simulations in explicit solvent.

548   The molecules were solvated in a theoretical box of explicit TIP3P waters and the solute atoms were

549   positioned at least at 10 Å from the solvent box edge. The equilibration phase consisted on energy

550   minimization of the solvent followed by an energy minimization of the entire system without restraints.

551   The system was then heated up to 300 K during 100 ps followed by 2 ns dynamics at constant

552   temperature of 300 K, controlled by the Langevin thermostat, and constant pressure of 1 atm. During

553   the simulations, the SHAKE algorithm was turned on and applied to all hydrogen atoms (41). A cut-

554   off of 8 Å for all non-bonded interactions was adopted. An integration time step of 2 fs was employed

555   and periodic boundaries conditions were applied throughout. During the simulations, the particle mesh

556   Ewald (PME) method was used to compute long-range electrostatic interactions (42-44). Minimization,

557   equilibration, and production phases were carried out by the pmemd.cuda module of AMBER 12 and

558   16, while the analyses of the simulations were performed using cpptraj module from AMBERTOOLS

559   16 (45-47). Data processing and 2D plots were carried out using GNUplot softwares.

560   4.14 Docking studies

561   The MenX (DP6) hexasaccharide was built as already explained for DP2 and DP12. The global

562   minimum conformer obtained from the analysis of DP2 and DP12 was taken as starting point for DP6

563   geometry. The molecule was then solvated in a theoretical box of explicit TIP3P waters, and the solute

564 atoms were positioned at least at 10 Å from the solvent box edge and counter ions were added to
565 maintain electroneutrality. The equilibration phase consisted on, first, an energy minimization of the
566 solvent followed by an energy minimization of the entire system without restraints, using the steepest
567 descent algorithm. The resulting structure was placed into the CRD of the IgG2a antibody and manually
568 docked to maximize the intermolecular interactions. The docked structures were then submitted to
569 energy minimization with a low gradient convergence threshold (0.05) in 5000 steps. The OPLS_2005
570 force field was employed, as integrated in the MAESTRO (Schroedinger) suite of programs.

571 All figures were generated using the molecular graphic software PyMOL (The PyMOL Molecular
572 Graphics System, Version 2.4 Schrödinger, LLC, http://www.pymol.org).

4.15 Protein crystallization

574 We set a series of crystallization conditions enzymatic or recombinant Fab with different OS lengths
575 and determined the following optimal crystallization conditions. Crystals of recombinant Fab in
576 complex with OS DP4 or DP5/6 were screened in a PACT premier™ (Molecular Dinamics)
577 crystallization screen. Crystals were obtained in 0.2 M Potassium thiocyanate; 0.1 M Bis-Tris propane;
578 pH6.5; 20% PEG 3350 Pact. Next, the crystals were soaked in cryosolvent 0,2 M Potassium
579 thiocyanate; 0,1 M Bis-Tris propane; pH6,5; 27% PEG 3350 + 10% Glycerol and immediately quench
580 cooled in liquid nitrogen prior to data collection.

581 X-ray diffraction data were collected at the SOLEIL Synchrotron (Soleil, France), on beamline
582 PROXIMA 2A (PX2-A), and using a EIGER X 9M detector. Data were indexed and processed using
583 XDS (48) and the CCP4 program suite (49). The structure of the complex was determined by molecular
584 replacement in Phaser (50), using as template model coordinates from the structure of mouse Fab
585 vFP05.01 (PDB code 5TKK). Refinement and manual model building were performed using Phenix
586 (51) and COOT (52). Structure quality was assessed using (PDB entry code D7OO2). Figures were
587 generated using PyMOL (http://www.pymol.org). Data collection and refinement statistics are reported
588 in Table S4, Supplemental Information) (53).

4.16 *In vivo* studies

590 Protocols were approved by the Italian Ministry of Health (Approval number n. 804/2015-PR). All
591 mice were housed under specific pathogen-free conditions at the GSK Vaccines Animal Resource
592 Center in compliance with the relevant guidelines (Italian Legislative Decree n 26/2014). Three groups
593 of eight female BALB/c mice were immunized by subcutaneous injection of glycoconjugates at 1 µg
594 dose in saccharide content using alum phosphate as an adjuvant. Mice received the vaccines at days 1,
595 14 and 28. Sera were bled at days 0, 27 and 42.

Figures

597 Frontiers requires figures to be submitted individually, in the same order as they are referred to in the
598 manuscript. Figures will then be automatically embedded at the bottom of the submitted manuscript.
599 Kindly ensure that each table and figure is mentioned in the text and in numerical order. Figures must

600 be of sufficient resolution for publication (see here for examples and minimum requirements).
601 Figures which are not according to the guidelines will cause substantial delay during the production
602 process. Figure legends should be placed at the end of the manuscript. Please see here for full Figure
603 guidelines
604

Conflict of Interest

606 MT, BB, DO, PH, MRR and RA are employees of GSK group of companies. MRR and RA are
607 inventors of patents related to this topic. The remaining authors declare that the research was conducted
608 in the absence of any commercial or financial relationships that could be construed as a potential
609 conflict of interest.

Author Contributions

611 GP, JB, JJB, TLR, SJ and RA conceived the work; GP, MT, BB, DO, SR, PH, IC, VI, SM, KM, BL,
612 SB, LU, EB, JR, MMR executed the work; GP, JB, TLR and RA wrote the manuscript; all contributed
613 to the manuscript.

Funding

Figure legends

622 **Figure 1. Specificity and bactericidal functionality of the supernatants from the hybridoma cells
623 producing mAb MenX.01 against MenX polysaccharide.** A) MenX immunization protocol. B)
624 Cross specificity test of purified MenX.01 mAb on ELISA plates coated with: i) MenX-PS, ii) i) MenA-
625 PS, iii) GBSII-PS, iv) MenX-CRM$_{197}$ conjugate and v) CRM$_{197}$ protein. C) MenX-CRM$_{197}$ molecules
626 were detected by western blot/imunoblot using MenX.01 mAb followed by anti-mouse Fab-HRP. As
627 a negative control, CRM$_{197}$ and GBSII-CRM$_{197}$ were used.

628 **Figure 2. In silico conformational studies on MenX CPS.** A) Glycosydic linkage analysis for DP2.
629 The φ/ψ and α/β plots from 1 µs MD simulations in explicit water are shown (GLYCAM06 force field)
630 for MenX DP2. The conformational flexibility at β is evident, while the other three torsion angles
631 display more restricted motion. B) Structure of the global minimum for MenX DP2 as determined by
632 MD calculations. C) Selected φ/ψ and α/β plots for different contiguous disaccharide fragments of
633 MenX DP12 from the 1µs MD simulations in explicit water (GLYCAM06) carried out for the
634 dodecasaccharide.

635 **Figure 3. Identification of the MenX Antigenic Determinant by Competitive ELISA and SPR.** A)
636 Purification of different length MenX OS fragments. Sepharose Q column chromatography of
637 depolymerized MenX CPS. B) MenX.01 inhibition ELISA using different length inhibitors. Different
638 MenX fragments were used as inhibitors, MenX CPS and PFT buffer were used as positive and
639 negative control, respectively. C) SPR Kinetic analysis of the MenX.01. binding kinetics and affinity
640 constants of MenX.01 to MenX-CRM$_{197}$ were determined by serial dilutions of the test antibody
641 MenX.01. D) Comparison of MenX CPS, DP5.5 and DP2 relative capacity to block MenX.01 antibody
642 binding by competitive SPR Study. Total capsular polysaccharide MenX DPS blocking was set at
643 100%.

644 **Figure 4. STD NMR (D2O, 600 MHz) of a DP7 fragment in complex with MenX0.1 mAb**. A) ^{1}H
645 NMR of the oligosaccharide in the presence of MenX0.1 mAb (50:1 molar ratio). B) The STD NMR
646 spectrum obtained for the complex upon on-resonance irradiation at 7 ppm; C) The STD NMR
647 spectrum obtained for the complex upon on-resonance irradiation at 8 ppm. All sugar ring protons
648 display transfer of saturation, with higher relative intensities for positions H-1 and H-4.

649 **Figure 5. Docking of DP6 with MenX.01 Fab.** A) Top and B) side view of the docking pose. The
650 DP6 engages the mAb binding pocket from the heavy to the light chains in the CRD**.** C) Detailed
651 intermolecular interactions in the docked-minimized structure of complex between MenX.01 Fab and
652 MenX DP6 OS. The amino acids that contribute to the binding are indicated.

653 **Figure 6. Immunogenicity of different length MenX OS conjugated to CRM$_{197}$**. IgG and SBA titers
654 measured after the second and third dose are reported. Data are obtained from immunization of eight
655 female BALB/c mice by subcutaneous injection of glycoconjugates at 1 µg dose in saccharide content
656 using alum phosphate as an adjuvant. Mice received the vaccines at days 1, 14 and 28. Sera were bled
657 at days 0, 27 and 42. Dot represent single mice serum. Statistics was calculated with Mann-Withney.

658

References

660 1.   Morelli L, Cancogni D, Tontini M, Nilo A, Filippini S, Costantino P, et al. Synthesis and
661 immunological evaluation of protein conjugates of Neisseria meningitidis X capsular polysaccharide
662 fragments. Beilstein J Org Chem. (2014) 10:2367-76.

663 2.   Fiebig T, Romano MR, Oldrini D, Adamo R, Tontini M, Brogioni B, et al. An efficient cell
664 free enzyme-based total synthesis of a meningococcal vaccine candidate. NPJ Vaccines. (2016)
665 1:16017.

666 3.   Ji X, Yao PP, Zhang LY, Li Y, Xu F, Mei LL, et al. Capsule switching of Neisseria
667 meningitidis sequence type 7 serogroup A to serogroup X. J Infect. (2017) 756:521-31.

668 4.   Micoli F, Romano MR, Tontini M, Cappelletti E, Gavini M, Proietti D, et al. Development of
669 a glycoconjugate vaccine to prevent meningitis in Africa caused by meningococcal serogroup X.
670 Proc Natl Acad Sci U S A. (2013) 11047:19077-82.

18

671   5.   Oldrini D, Fiebig T, Romano MR, Proietti D, Berger M, Tontini M, et al. Combined
672   Chemical Synthesis and Tailored Enzymatic Elongation Provide Fully Synthetic and Conjugation-
673   Ready Neisseria meningitidis Serogroup X Vaccine Antigens. ACS Chem Biol. (2018) 134:984-94.

674   6.   Chen WH, Neuzil KM, Boyce CR, Pasetti MF, Reymann MK, Martellet L, et al. Safety and
675   immunogenicity of a pentavalent meningococcal conjugate vaccine containing serogroups A, C, Y,
676   W, and X in healthy adults: a phase 1, single-centre, double-blind, randomised, controlled study.
677   Lancet Infect Dis. (2018) 1810:1088-96.

678   7.   Muindi KM, McCarthy PC, Wang T, Vionnet J, Battistel M, Jankowska E, et al.
679   Characterization of the meningococcal serogroup X capsule N-acetylglucosamine-1-
680   phosphotransferase. Glycobiology. (2014) 242:139-49.

681   8.   Lee D, Kim EJ, Kilgore PE, Takahashi H, Ohnishi M, Tomono J, et al. A Novel Loop-
682   Mediated Isothermal Amplification Assay for Serogroup Identification of Neisseria meningitidis in
683   Cerebrospinal Fluid. Front Microbiol. (2015) 6:1548.

684   9.   Pizza M, Rappuoli R. Neisseria meningitidis: pathogenesis and immunity. Curr Opin
685   Microbiol. (2015) 23:68-72.

686   10.   Fiebig T, Berti F, Freiberger F, Pinto V, Claus H, Romano MR, et al. Functional expression
687   of the capsule polymerase of Neisseria meningitidis serogroup X: a new perspective for vaccine
688   development. Glycobiology. (2014) 242:150-8.

689   11.   Harale KR, Dumare NB, Singh D, Misra AK, Chhikara MK. Synthesis of a tetrasaccharide
690   and its glycoconjugate corresponding to the capsular polysaccharide of Neisseria meningitidis
691   serogroup X and its immunochemical studies. Rsc Adv. (2015) 552:41332-40.

692   12.   Ming SA, Cottman-Thomas E, Black NC, Chen Y, Veeramachineni V, Peterson DC, et al.
693   Interaction of Neisseria meningitidis Group X N-acetylglucosamine-1-phosphotransferase with its
694   donor substrate. Glycobiology. (2018) 282:100-7.

695   13.   Fallarini S, Buzzi B, Giovarruscio S, Polito L, Brogioni G, Tontini M, et al. A Synthetic
696   Disaccharide Analogue from Neisseria meningitidis A Capsular Polysaccharide Stimulates Immune
697   Cell Responses and Induces Immunoglobulin G (IgG) Production in Mice When Protein-Conjugated.
698   ACS Infect Dis. (2015) 110:487-96.

699   14.   Hlozek J, Kuttel MM, Ravenscroft N. Conformations of Neisseria meningitidis serogroup A
700   and X polysaccharides: The effects of chain length and O-acetylation. Carbohydr Res. (2018) 465:44-
701   51.

702   15.   Pecetta S, Tontini M, Faenzi E, Cioncada R, Proietti D, Seubert A, et al. Carrier priming
703   effect of CRM197 is related to an enhanced B and T cell activation in meningococcal serogroup A
704   conjugate vaccination. Immunological comparison between CRM197 and diphtheria toxoid. Vaccine.
705   (2016) 3420:2334-41.

706   16.   Trotter CL, Lingani C, Fernandez K, Cooper LV, Bita A, Tevi-Benissan C, et al. Impact of
707   MenAfriVac in nine countries of the African meningitis belt, 2010-15: an analysis of surveillance
708   data. Lancet Infect Dis. (2017) 178:867-72.

709   17.   Tanir G, Ozsurekci Y, Lucidarme J, Yasar Durmus S, Lekshmi A, Akisoglu O, et al.
710   Neisseria meningitidis Serogroup X ST-5799 (ST-22 complex) in Turkey: A unique pediatric case.
711   Hum Vaccin Immunother. (2018) 141:209-12.

712   18.   Garrido R, Puyada A, Fernandez A, Gonzalez M, Ramirez U, Cardoso F, et al. Quantitative
713   proton nuclear magnetic resonance evaluation and total assignment of the capsular polysaccharide
714   Neisseria meningitidis serogroup X. J Pharm Biomed Anal. (2012) 70:295-300.

715   19.   Smith ICP. Determination of Composition, Sequence, and Conformation of Immunological
716   Polysaccharides by C-13 Nuclear Magnetic-Resonance. T New York Acad Sci. (1974) 366:593-.

717   20.   Carboni F, Angiolini F, Fabbrini M, Brogioni B, Corrado A, Berti F, et al. GBS type III
718   oligosaccharides containing a minimal protective epitope can be turned into effective vaccines by
719   multivalent presentation. J Infect Dis. (2019) 2216.

720   21.   Oldrini D, Del Bino L, Arda A, Carboni F, Henriques P, Angiolini F, et al. Structure-Guided
721   Design of a Group B Streptococcus Type III Synthetic Glycan-Conjugate Vaccine. Chemistry. (2020)
722   2631:6944.

723   22.   Soliman C, Pier GB, Ramsland PA. Antibody recognition of bacterial surfaces and
724   extracellular polysaccharides. Curr Opin Struct Biol. (2020) 62:48-55.

725   23.   Broecker F, Hanske J, Martin CE, Baek JY, Wahlbrink A, Wojcik F, et al. Multivalent
726   display of minimal Clostridium difficile glycan epitopes mimics antigenic properties of larger
727   glycans. Nat Commun. (2016) 7.

728   24.   Schumann B, Reppe K, Kaplonek P, Wahlbrink A, Anish C, Witzenrath M, et al.
729   Development of an Efficacious, Semisynthetic Glycoconjugate Vaccine Candidate against
730   Streptococcus pneumoniae Serotype 1. Acs Central Sci. (2018) 43:357-61.

731   25.   Carboni F, Adamo R, Fabbrini M, De Ricco R, Cattaneo V, Brogioni B, et al. Structure of a
732   protective epitope of group B Streptococcus type III capsular polysaccharide. P Natl Acad Sci USA.
733   (2017) 11419:5017-22.

734   26.   Acevedo R, Zayas C, Norheim G, Fernandez S, Cedre B, Aranguren Y, et al. Outer
735   membrane vesicles extracted from Neisseria meningitidis serogroup X for prevention of
736   meningococcal disease in Africa. Pharmacol Res. (2017) 121:194-201.

737   27.   Bundle DR, Smith ICP, Jennings HJ. Determination of Structure and Conformation of
738   Bacterial Polysaccharides by Carbon 13 Nuclear Magnetic-Resonance - Studies on Group-Specific
739   Antigens of Neisseria-Meningitidis Serogroups a and X. J Biol Chem. (1974) 2497:2275-81.

740   28.   Salomon-Ferrer R, Case DA, Walker RC. An overview of the Amber biomolecular simulation
741   package. Wires Comput Mol Sci. (2013) 32:198-210.

742   29.   M. J. Frisch GWT, H. B. Schlegel, G. E. Scuseria, M. A. Robb, J. R. Cheeseman, G.
743   Scalmani, V. Barone, G. A. Petersson, H. Nakatsuji, X. Li, M. Caricato, A. Marenich, J. Bloino, B.
744   G. Janesko, R. Gomperts, B. Mennucci, H. P. Hratchian, J. V. Ortiz, A. F. Izmaylov, J. L.
745   Sonnenberg, D. Williams-Young, F. Ding, F. Lipparini, F. Egidi, J. Goings, B. Peng, A. Petrone, T.
746   Henderson, D. Ranasinghe, V. G. Zakrzewski, J. Gao, N. Rega, G. Zheng, W. Liang, M. Hada, M.
747   Ehara, K. Toyota, R. Fukuda, J. Hasegawa, M. Ishida, T. Nakajima, Y. Honda, O. Kitao, H. Nakai, T.
748   Vreven, K. Throssell, J. A. Montgomery, Jr., J. E. Peralta, F. Ogliaro, M. Bearpark, J. J. Heyd, E.
749   Brothers, K. N. Kudin, V. N. Staroverov, T. Keith, R. Kobayashi, J. Normand, K. Raghavachari, A.
750   Rendell, J. C. Burant, S. S. Iyengar, J. Tomasi, M. Cossi, J. M. Millam, M. Klene, C. Adamo, R.
751   Cammi, J. W. Ochterski, R. L. Martin, K. Morokuma, O. Farkas, J. B. Foresman, and D. J. Fox.
752   Gaussian 09, Revision A.01. Gaussian, Inc, Wallingford CT; (2016).   20

753   30.   Sharma N, Hanif S, Rana R, Upadhyay D, Chhikara MK. Evaluation of impact of temperature
754   and pH alterations on the size and antigenicity of meningococcal serogroup A and X polysaccharides
755   and conjugates. Vaccine. (2019) 377:965-72.

756   31.   Schrödinger Release 2021-1: Maestro. New York, NY: Schrödinger, LLC; (2021).

757   32.   Reyes F, Otero O, Camacho F, Amin N, Ramirez F, Valdes Y, et al. A novel monoclonal
758   antibody to Neisseria meningitidis serogroup X capsular polysaccharide and its potential use in
759   quantitation of meningococcal vaccines. Biologicals. (2014) 426:312-5.

760   33.   Uddin S, Borrow R, Haeney MR, Moran A, Warrington R, Balmer P, et al. Total and
761   serotype-specific pneumococcal antibody titres in children with normal and abnormal humoral
762   immunity. Vaccine. (2006) 2427-28:5637-44.

763   34.   Richter MY, Jakobsen H, Birgisdottir A, Haeuw JF, Power UF, Del Giudice G, et al.
764   Immunization of female mice with glycoconjugates protects their offspring against encapsulated
765   bacteria. Infect Immun. (2004) 721:187-95.

766   35.   Findlow J, Balmer P, Borrow R. A review of complement sources used in serum bactericidal
767   assays for evaluating immune responses to meningococcal ACWY conjugate vaccines. Hum Vaccin
768   Immunother. (2019) 1510:2491-500.

769   36.   Lee CJ, Lee LH, Frasch CE. Protective immunity of pneumococcal glycoconjugates. Crit Rev
770   Microbiol. (2003) 294:333-49.

771   37.   Madariaga S, Cedré B, García M, González E, Valerie Anne Ferro, R A. Evaluation of
772   Bactericidal Activity of Monoclonal Antibodies Obtained from Neisseria meningitidis. Clinical
773   Infectious Diseases: Open Access. (2018 (January 2019)) 2:3:2-5.

774   38.   Haji-Ghassemi O, Blackler RJ, Martin Young N, Evans SV. Antibody recognition of
775   carbohydrate epitopesdagger. Glycobiology. (2015) 259:920-52.

776   39.   Andrew SM, Titus JA. Fragmentation of immunoglobulin G. Curr Protoc Cell Biol. (2003)
777   Chapter 16:Unit 16 4.

778   40.   Giuliani MM, Santini L, Brunelli B, Biolchi A, Arico B, Di Marcello F, et al. The region
779   comprising amino acids 100 to 255 of Neisseria meningitidis lipoprotein GNA 1870 elicits
780   bactericidal antibodies. Infect Immun. (2005) 732:1151-60.

781   41.   Miyamoto S, Kollman PA. Settle - an Analytical Version of the Shake and Rattle Algorithm
782   for Rigid Water Models. J Comput Chem. (1992) 138:952-62.

783   42.   Darden T, York D, Pedersen L. Particle Mesh Ewald - an N.Log(N) Method for Ewald Sums
784   in Large Systems. Journal of Chemical Physics. (1993) 9812:10089-92.

785   43.   Essmann U, Perera L, Berkowitz ML, Darden T, Lee H, Pedersen LG. A Smooth Particle
786   Mesh Ewald Method. Journal of Chemical Physics. (1995) 10319:8577-93.

787   44.   Crowley MF, Darden TA, Cheatham TE, Deerfield DW. Adventures in improving the scaling
788   and accuracy of a parallel molecular dynamics program. J Supercomput. (1997) 113:255-78.

789   45.   Le Grand S, Gotz AW, Walker RC. SPFP: Speed without compromise-A mixed precision
790   model for GPU accelerated molecular dynamics simulations. Comput Phys Commun. (2013)
791   1842:374-80.

792   46.   Gotz AW, Williamson MJ, Xu D, Poole D, Le Grand S, Walker RC. Routine Microsecond
793   Molecular Dynamics Simulations with AMBER on GPUs. 1. Generalized Born. J Chem Theory
794   Comput. (2012) 85:1542-55.

795   47.   Salomon-Ferrer R, Gotz AW, Poole D, Le Grand S, Walker RC. Routine Microsecond
796   Molecular Dynamics Simulations with AMBER on GPUs. 2. Explicit Solvent Particle Mesh Ewald. J
797   Chem Theory Comput. (2013) 99:3878-88.

798   48.   Kabsch W. Xds. Acta Crystallogr D. (2010) 66:125-32.

799   49.   Winn MD, Ballard CC, Cowtan KD, Dodson EJ, Emsley P, Evans PR, et al. Overview of the
800   CCP4 suite and current developments. Acta Crystallographica Section D-Structural Biology. (2011)
801   67:235-42.

802   50.   Mccoy AJ, Grosse-Kunstleve RW, Adams PD, Winn MD, Storoni LC, Read RJ. Phaser
803   crystallographic software. J Appl Crystallogr. (2007) 40:658-74.

804   51.   Liebschner D, Afonine PV, Baker ML, Bunkoczi G, Chen VB, Croll TI, et al.
805   Macromolecular structure determination using X-rays, neutrons and electrons: recent developments
806   in Phenix. Acta Crystallographica Section D-Structural Biology. (2019) 75:861-77.

807   52.   Emsley P, Cowtan K. Coot: model-building tools for molecular graphics. Acta
808   Crystallographica Section D-Structural Biology. (2004) 60:2126-32.

809   53.   Williams CJ, Headd JJ, Moriarty NW, Prisant MG, Videau LL, Deis LN, et al. MolProbity:
810   More and better reference data for improved all-atom structure validation. Protein Sci. (2018)
811   271:293-315.

812

Figure 1.TIF

A

Immunization schedule

Figure 2.TIF

Figure 3.TIF

A — MenX OS production

B — Competitive ELISA

C — SPR

D — Competitive SPR

Figure 4.TIF

Figure 5.TIF

A

CRD Light chain | CRD Heavy chain
Light chain | Heavy chain

Front view

B

Top view

C

Heavy chain
Light chain

Figure 6.TIF

A
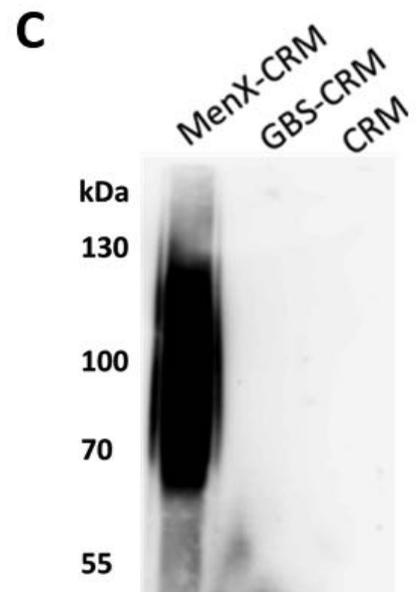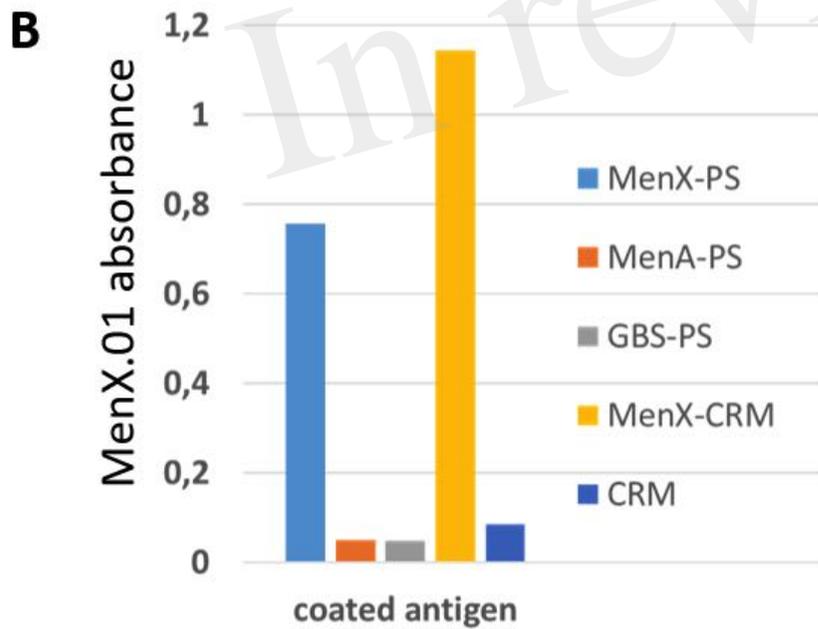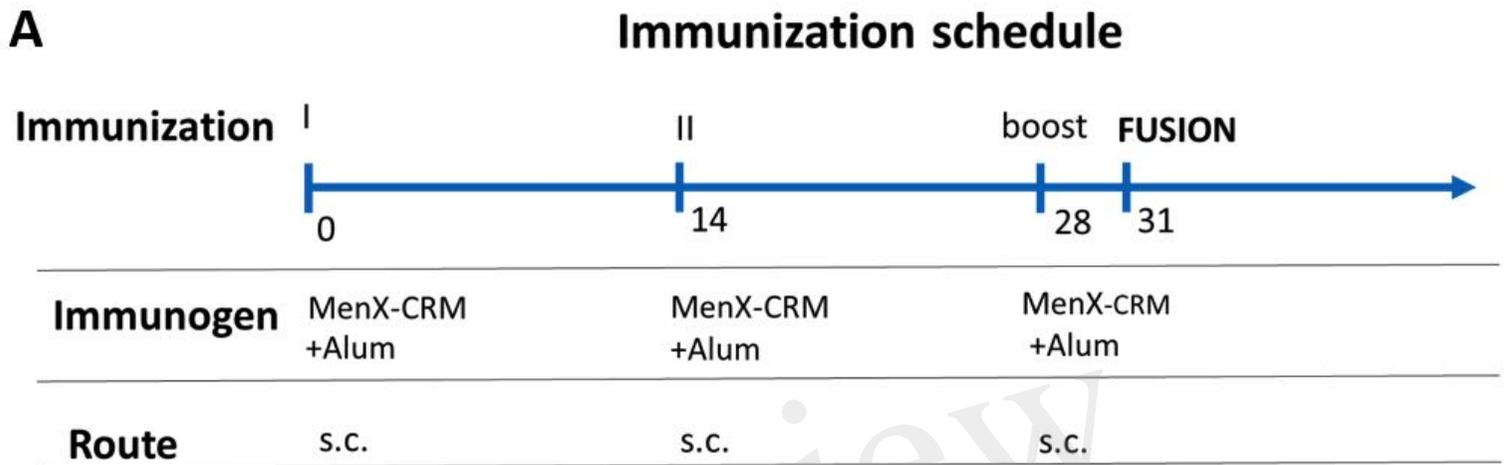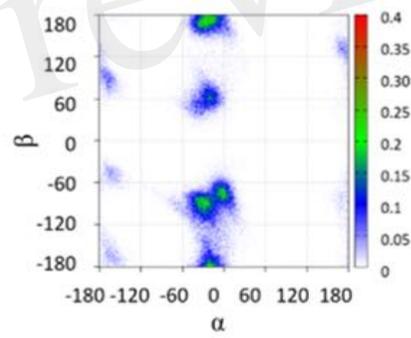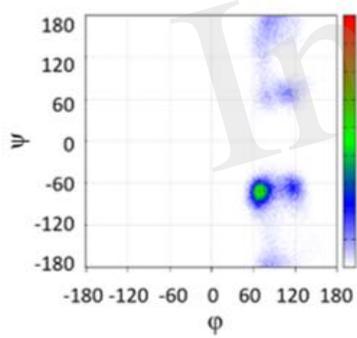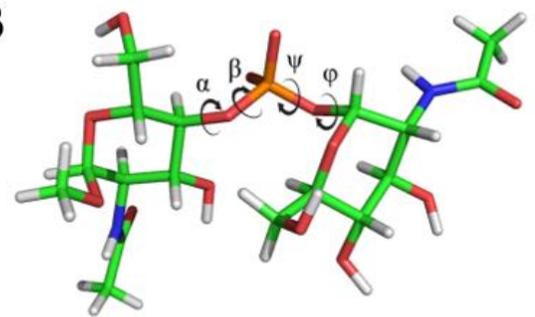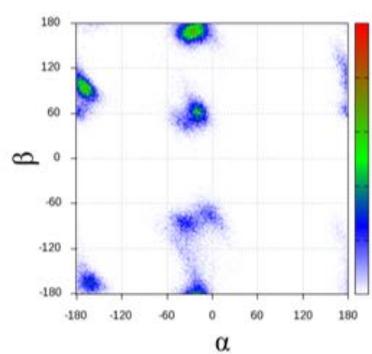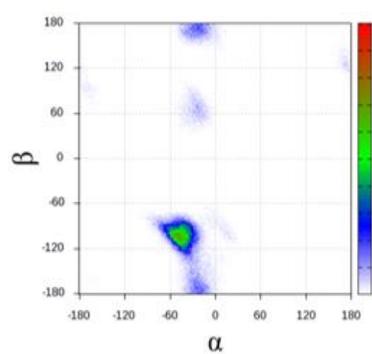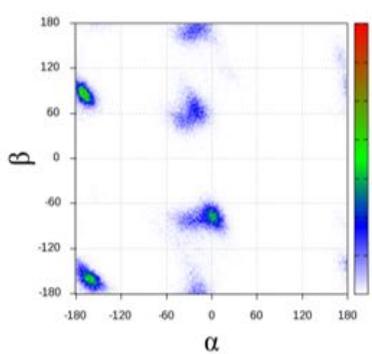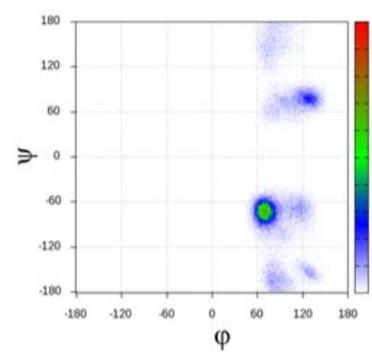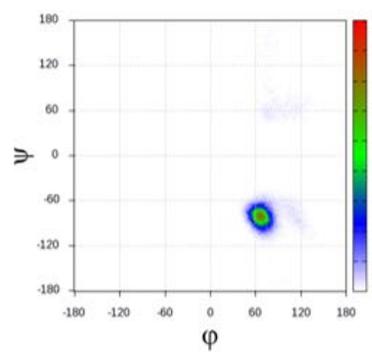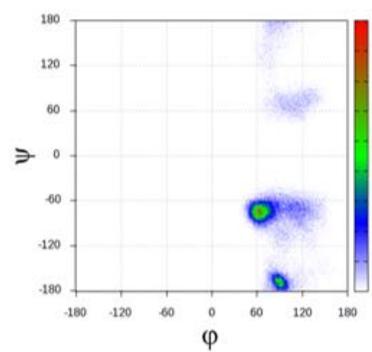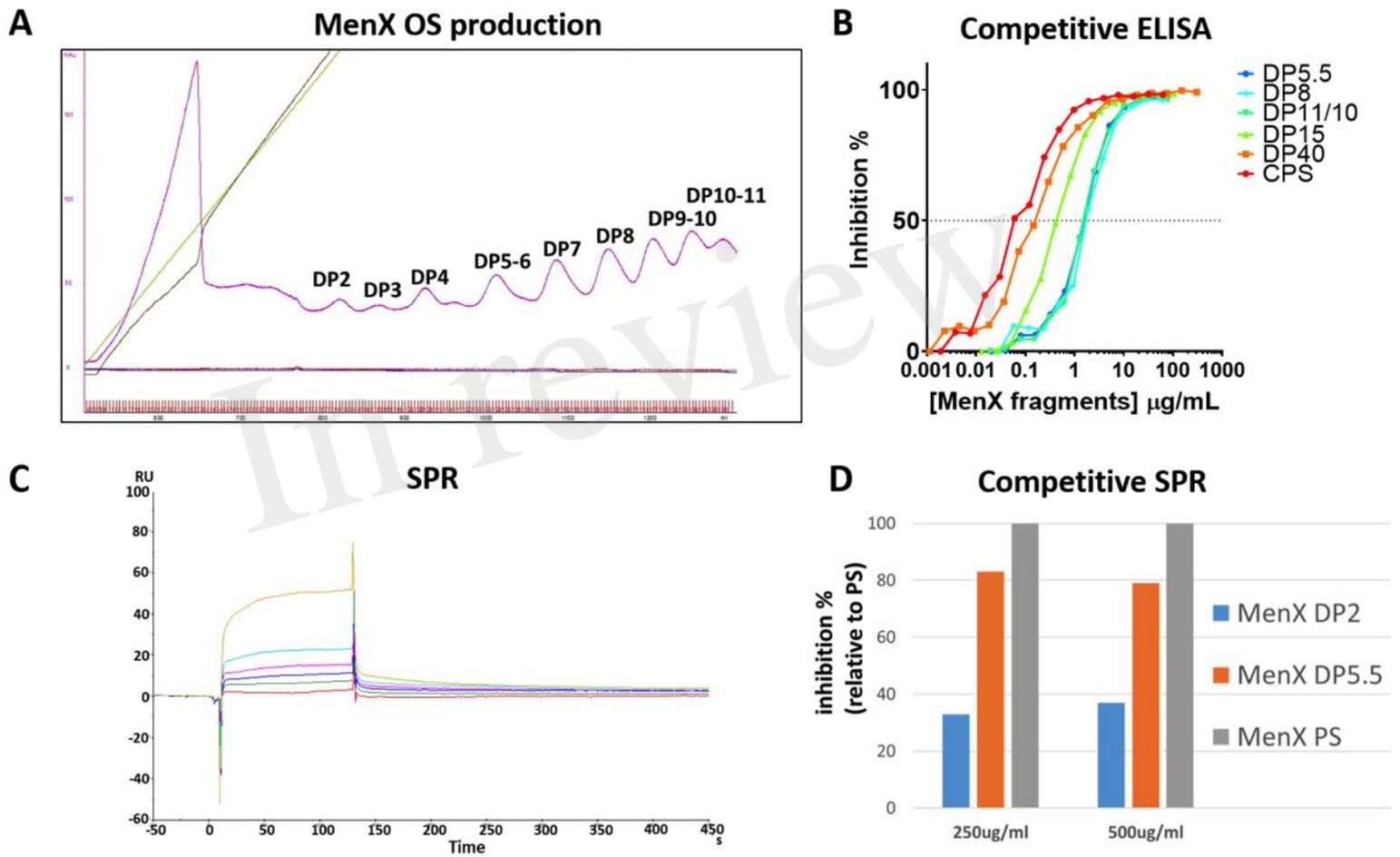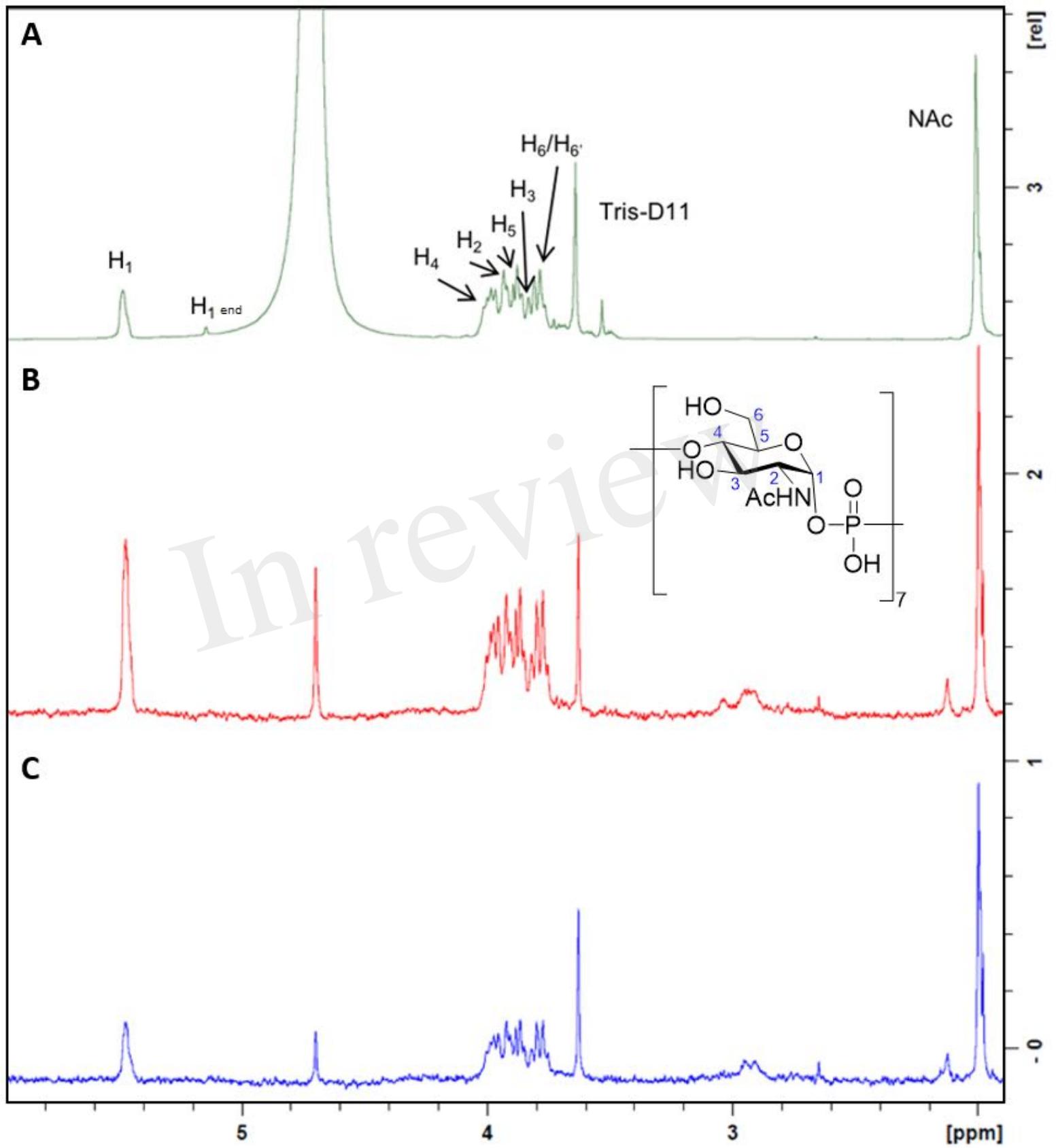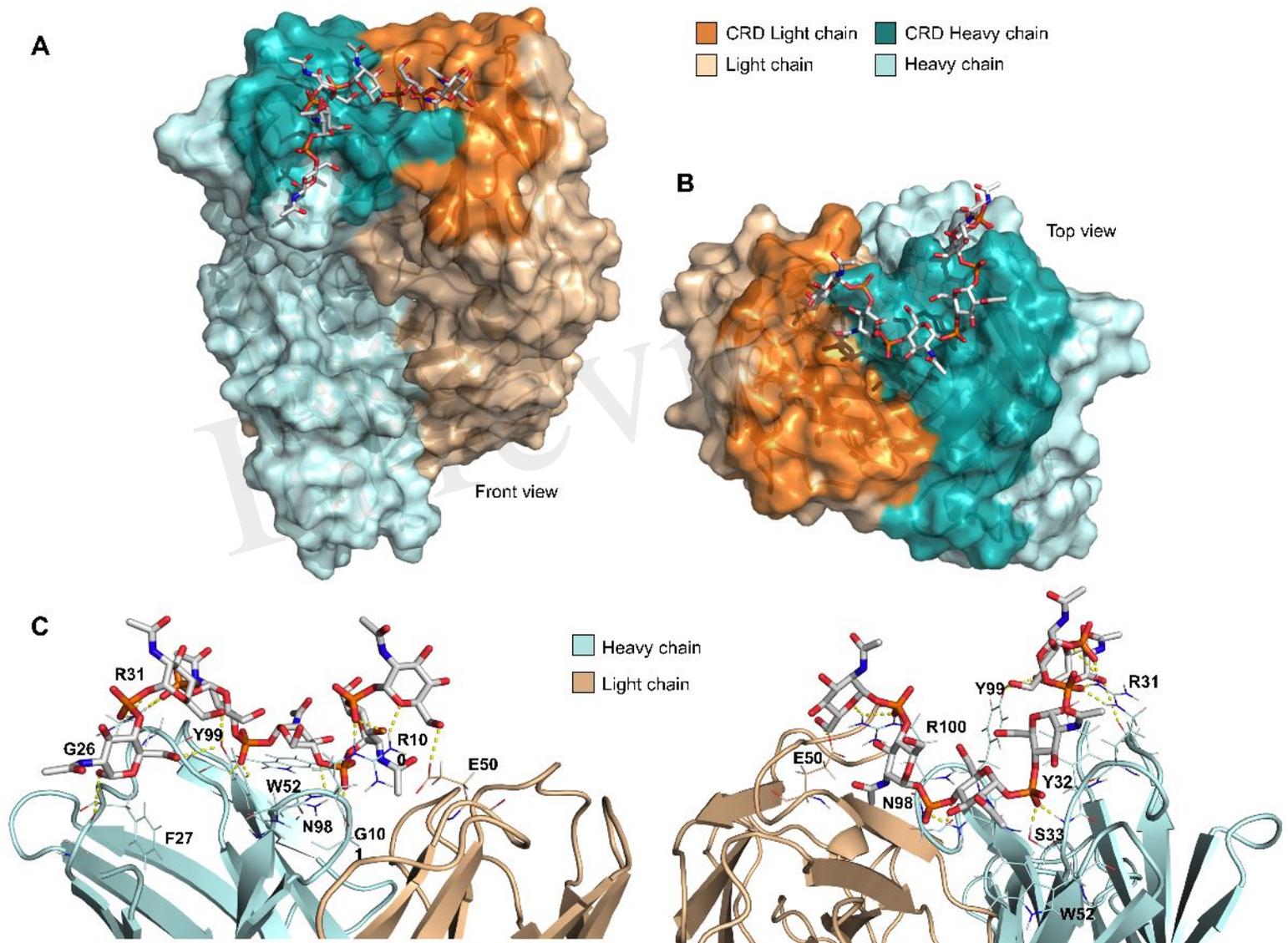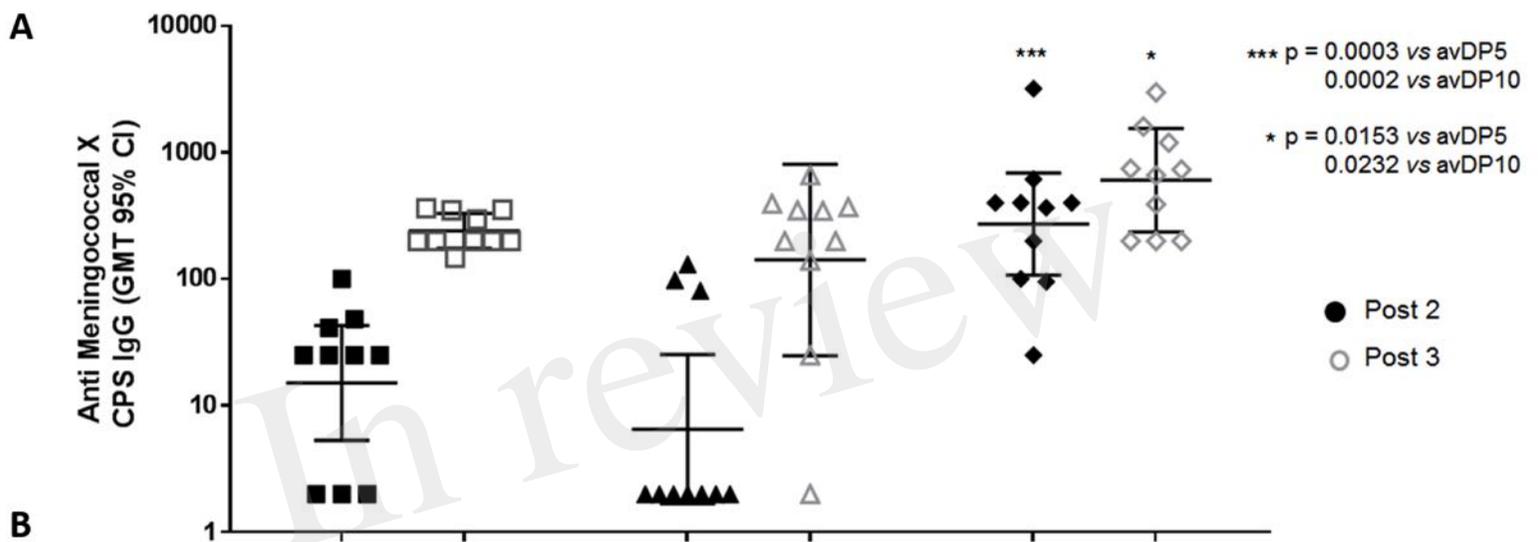
B

rSBA (MenX Z9516 strain)	MenX-CRM$_{197}$ avDP5	MenX-CRM$_{197}$ avDP10	MenX-CRM$_{197}$ avDP20
Post 2	64	32	1024
Post 3	1024	1024	8192